Langmuir

Article

pubs.acs.org/Langmuir

Aragonite Crystals Grown on Bones by Reaction of CO_2 with Nanostructured $Ca(OH)_2$ in the Presence of Collagen. Implications in Archaeology and Paleontology

Irene Natali,[†] Paolo Tempesti,[†] Emiliano Carretti,[†] Mariangela Potenza,[†] Stefania Sansoni,[‡] Piero Baglioni,[†] and Luigi Dei*[,†]

[†]Department of Chemistry "Ugo Schiff" and CSGI Consortium, University of Florence, via della Lastruccia 3, 50019 Sesto Fiorentino (FI), Italy

Supporting Information

ABSTRACT: The loss of mechanical properties affecting archeological or paleontological bones is often caused by demineralization processes that are similar to those driving the mechanisms leading to osteoporosis. One simple way to harden and to strengthen demineralized bone remains could be the *in situ* growth of $CaCO_3$ crystals in the aragonite polymorph − metastable at atmospheric pressure −which is known to have very strong mechanical strength in comparison with the stable calcite. In the present study the controlled growth of aragonite crystals was achieved by reaction between atmospheric CO_2 and calcium hydroxide nanoparticles in the presence of collagen within the deteriorated bones. In a few days the carbonation of $Ca(OH)_2$ particles led to a mixture of calcite and aragonite, increasing the strength of the mineral network of the bone. Scanning electron microscopy coupled with energy dispersive X-ray spectroscopy (SEM−EDS) and Fourier transform infrared (FT-IR) spectrometry showed that aragonite crystallization was achieved. The effect of the aragonite crystal formation on the mechanical properties of the deteriorated bones was investigated by means of X-rays microtomography, helium porosimetry, atomic force microscopy (AFM), and Vickers microhardness techniques. All these data enabled to conclude that the strength of the bones increased of a factor of 50−70% with respect to the untreated bone. These results could have immediate impact for preserving archeological and paleontological bone remains.

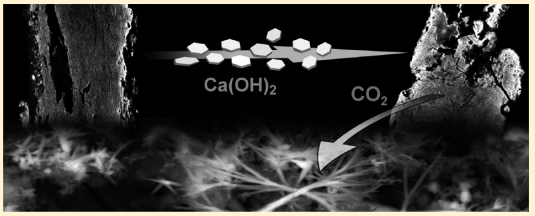

INTRODUCTION

The study of bone preservation is intimately connected to the understanding of their structural characteristics and their chemical composition. Macroscopically, bones are constituted of two superimposed tissues having almost the same chemical composition: a dense outer layer, the cortical bone, surrounds an inner one, more porous and less dense (*spongiosa*).[1] A bone in general is a complex material in which each constituent is organized in a hierarchical structure: fibrous, laminar, particulate, and porous structures are present at different size scales.[2] The three main chemical components of bones are collagen type I, that constitutes about 90% of the organic matter (there are also the so-called noncollageneous proteins, NCPs), dahallite (carbonated apatite, $Ca_5(PO_4, CO_3)_3$ (OH)), and water. Mineralized collagen fibrils are the building block of bones: the fibrous nature of collagen allows platelet-shaped crystals of dahallite to crystallize in the three-dimensional matrix conferring strength and hardness to the bone tissue.[3] The intercalation of the mineral and organic components occurs at nano-, micro-, and mesoscale providing, respectively, strength and elasticity.[4] Then, mechanical properties of bones are strongly related to their architecture: Currey showed that elastic properties of bones depend on calcium content and on porosity.[5] In particular, Young's modulus increases monotonically with Ca content and inversely with porosity. An interesting review has been made by Weiner and Wagner, in which authors investigate the structure−function relations for each hierarchical level of organization underlying the related mechanical implications.[3]

It is well-known that osteoporosis is a disease characterized by the reduction of bone mineral density, a lowering of the bone mass, and the deterioration of bone microarchitecture and tissue. These conditions lead to bone fragility and high risk of fracture. Bone mass density (BMD) is investigated in medicine by means of several techniques such as dual energy X-ray absorptiometry (DXA), single energy X-ray absorptiometry (SXA), and quantitative computed tomography (QTC).[6] In order to prevent osteoporosis a calcium rich diet is recommended, while pharmacological therapies provide estrogens, progestinals and bisphosphonates as well as hormones.[6] Even if osteoporosis affects living creatures, a decrease in bone mass also occurs in archeological skeletons representing the main cause of damage of these kinds of finds. Gonzalez-Reimers et al.[7] examined the value of bone density by QCT in prehistoric bones for the diagnosis of osteopenia in skeletal remains, highlighting the limits affecting this technique for the

Received: October 28, 2013
Revised: December 9, 2013
Published: January 10, 2014

study of these kinds of materials. Trabecular mineral density of archeological bones has been investigated by Farquharson et al.[8] that for the first time applied low angle X-ray scattering technique for this kind of study: the results have been compared with those obtained with other specific techniques such as dual energy X-ray absorptiometry and photodensitometry, as well as with bone mineral density values obtained by weighing and measuring the volume of the samples. With regard to bone mineral solubility, Berna et al.[9] identified a recrystallization window in order to define the conditions under which bone crystals dissolve and reprecipitate as a more insoluble form of carbonated hydroxyl apatite. Diagenetic changes and mineral alterations have been investigated by means of several techniques with the attempt to elucidate the mechanisms of preservation of archeological biomolecules.[10−14]

Nowadays, archeological and paleontological bones need to be saved, and consequently they may undergo conservation procedures such as cleaning and consolidating treatments. The fragility affecting archeological materials leads to the necessity to perform treatments aimed at hardening and strengthening them: vinyl and acrylic polymers have become the most popular consolidating agents employed, acting as a glue, filling tiny cracks and adhering smaller pieces of materials. Unfortunately, these may lead to undesired effects in terms of compatibility, reversibility, and stability.[15]

The aim of the present work was to study the carbonation process occurring between nanostructured calcium hydroxide and atmospheric carbon dioxide in the presence of promoting agents for the growth of the metastable polymorph aragonite. In particular, it was interesting to verify the conditions under which the formation of the aragonite carbonated phase which is known to possess excellent mechanical properties was achieved. Many authors indicate the possibility to modulate the crystallization of calcium carbonate polymorphs in the presence of metal ions,[16] as well as using collagenous matrices in association or not with magnesium ions.[17,18] It is known that auxiliary molecules may promote or inhibit crystal nucleation depending on their composition:[19] the effect of proteins (i.e., collagen) on the morphology of crystal growth has been described in terms of activation energy and variation in complementarity of various crystal faces and the organic substrate. It has been shown that the nucleation of an inorganic polymorph is controlled by the presence of an organic matrix, and activation energy can be influenced in three different ways (nonspecific nucleation catalysis, structure-specific nucleation, or a combination of both) involving thermodynamic and kinetic aspects.[20] Some authors have investigated both in nature and in the laboratory the controlled phase transition between aragonite and calcite in nacre with the use of soluble polyanionic proteins;[21,22] in this context, some works highlighted the possibility to enhance the crystallization of calcium carbonate in aragonite phase by tuning the concentration of many different organic compounds such as poly(L-aspartate) and gelatin[18] as well as collagen[23] in association or not with metal ions like Mg^{2+}.[17] Nevertheless, Gomez-Villalba et al.[24] demonstrated how $Ca(OH)_2$ nanocrystals can give the formation of aragonite even in the absence of collagen and Mg^{2+} ions. Although aragonite is the metastable phase under ambient conditions, it is well-known that many organisms overwork biological macromolecules to control aragonite nucleation, that is, calcium carbonated phase characterized by high mechanical strength:[25] as an example, aragonite mineral bridges inside the organic matrix of seashells absorb the bulk of the externally applied loads while the organic component provide toughness, preventing the propagation of cracks.[26] As a consequence of the above, $Ca(OH)_2$ nanoparticles appeared to be a possible precursor of aragonite calcium carbonate if associated with a protein containing matrix. Then, the scope was to enhance the formation of the metastable aragonite during $Ca(OH)_2$ carbonation by atmospheric CO_2 by exploiting the properties of collagen, present in the deteriorated bones, as aragonite-promoter. Implications for archeological and paleontological bone remains were also taken into account.

MATERIALS AND METHODS

Materials. Calcium hydroxide nanoparticles dispersed in 2-propanol 5.0 g/L (Nanorestore) were prepared by a size and shape controlled synthesis at the CSGI laboratories,[27−30] purchased by CTS, Altavilla Vicentina (VI), Italy, and used without further purification. Preventol RI 80 was supplied by Lanxess, Germany. 2-Propanol, acetone, and KBr were supplied by Merck, Darmstadt, Germany, and were used without any further purification. Water was purified by a Millipore Organex system ($R \geq 16$ MΩ cm). Bone fragments from the San Clemente's relics (Late Middle Ages) are owned by the parish church of "San Vittore Martire" (Lainate, Milan, Italy), and there conserved. They were made available in the frame of a scientific cooperation. After a collapse of the wooden structure onto which the shrine was placed, it was decided to perform a complete restoration of the whole complex, including garments and the shrine. Many decay processes were affecting S. Clemente's relics, but the priority objective was to recover the hardness and the cohesion of the bone remains: fragility and decohesion were indeed the main damage effects they were presenting and consolidation work was needed.

Bone Treatment. The skeleton from which the fragments were taken had been cleaned using acetone and disinfected by using Preventol RI 80. Then, the various parts of the skeleton were treated with 2-propanol by brush in order to facilitate the penetration of the consolidating agent and therefore immersed in Nanorestore pure or diluted (80/20 v/v%) in 2-propanol/water mixtures (90/10 v/v%); the imbibition method was chosen in order to achieve complete penetration of the dispersion in the entire volume of bones. The operation was repeated 10 times; every application was carried out after the complete evaporation of the solvent. All these operations were performed inside a room − used as conservation laboratory − of the church building where the relics were conserved with climate parameters similar to the ones from the church in which San Clemente's relics were kept, in order to maintain constant the environmental conditions and facilitate the carbonation process thanks to high values of relative humidity (around 75%). After three months, sampling of the fragments used for this study was carried out. The complete carbonation of calcium hydroxide nanoparticles was ascertained on all the fragments by FT-IR measurements.

X-ray Diffraction. Powder X-ray diffraction (XRD) measurements were carried out at CRIST Centre, University of Florence (Italy), using a Bruker D8 Advance diffractometer equipped with Cu Kα radiation and operating in $\theta-2\theta$ Bragg−Brentano geometry at 40 kV and 40 mA.

Microtomography. μ-CT data were collected using a Skyscan 1172 high-resolution MicroCT system at CRIST, University of Florence (Italy). This system has a sealed, microfocus tungsten X-ray tube with a 5 μm focal spot size. The X-rays were produced by exposing the anode to an electron beam at 59 kV at 167 μA. Each sample was placed on the pedestal between the X-ray source and the CCD detector and the 2D X-ray images were captured over 180° rotating the sample with a slice-to-slice rotation angle of 0.3°, each 2D image represents one slice. The total acquisition time was approximately 30 min. Spatial resolution of the images was kept in a range of 3 μm in terms of pixel size.

ESEM/SEM-EDS Analyses. Environmental scanning electron microscopy (ESEM) images were collected by means of a FEI Quanta 200 microscope coupled with an EDS (SUTW detector) at CE.M.E.

dx.doi.org/10.1021/la404085v | Langmuir 2014, 30, 660−668

(Centro di Microscopie Elettroniche), CNR of Florence. The dimensions of the microscope chamber are 20 × 15 cm, allowing the introduction of the full plates and avoiding the necessity of sample collection. The working distance was 10 mm and the acceleration potential 30 kV. Scanning electron microscopy (SEM) images were collected after metallization of the samples by means of a surface layer of carbon with a Zeiss EVO MA15 coupled with an EDS OXFORD INCA 250 at M.E.M.A. (Centro Interdipartimentale di Microscopia Elettronica e Microanalisi), University of Florence. The working distance was 10 mm and the acceleration potential 12 kV.

FT-IR Measurements. Fourier transform infrared spectroscopy measurements were carried out using a BioRad FTS-40 spectrometer in the range 4000−400 cm^{-1}. Spectra are averages of 128 scans recorded in absorbance mode with 2 cm^{-1} resolution. KBr pellets were prepared by finely grinding and mixing few samples in pure KBr.

Atomic Force Microscopy. The bone morphology was inspected by means of AFM on a XE-100E (Park System Corp., Korea) in noncontact mode using silicon tips (curvature radius <10 nm, force constant 40 N/m).

The root-mean-square roughness R_q corresponds to the standard deviation of the height values of the points of a selected region of an AFM micrograph; numerically, it corresponds to the values assumed by the z coordinate in a given area

$$R_q = \sqrt{\frac{\sum_{i=1}^{n} (z_i - \bar{z})}{n}}$$

where n is the number of points, z_i is the value of the z coordinate of the ith point, and $\bar{z}$ is the average height value in the selected area. For both T (treated) and NT (not treated) samples, the R_q value indicated in the text is the average of 30 measurements (3 measurements were carried out for each of the 10 AFM micrographs collected from both samples). An example of the procedure followed for R_q calculation is reported in Figure SI1.

Vickers Microhardness Measurements. The bone microhardness was evaluated with a HX-1000 TM (Remet s.a.s., Italy) microhardness tester with test load ranging from 10 to 1000 g and a load duration ranging from 5 to 60 s. The images were analyzed by means of AUTOVICKERS software. Vickers hardness tests were carried out at ambient temperature. For each test a square-based diamond pyramid was used as indenter; the applied loads were between 25 and 100 g, while the load time was fixed at 10 s.

Helium Porosimetry. Each sample was weighed and the volume was determined by means of mercury displacement method. Ten measurements were performed in order to get the mean value of each quantity; then, the apparent density of the two samples was calculated. A Helium Picnometer Accupyc II 1240 - Micromeritics (Centro di Geotecnologie, University of Siena) was used in order to determine the volume of the pores of each sample. Through the above-mentioned parameters, porosity values were obtained.

Ion Chromatography. This was performed using a DionexDX120 ionic chromatograph equipped with a Dionex CS12A column and using $Na_2CO_3/NaHCO_3$ 2.5 mM as eluent.

Amino Acid Analysis by Gas Chromatography Coupled with Mass Spectrometry (GC-MS). These measurements were carried out at the Getty Conservation Institute, Scientific Department. Two bone samples, A, not treated by nanolime, and B, treated by nanolime, were analyzed for proteins and oils by gas chromatography mass spectrometry (GC/MS). In order to determine the range of amino acid concentrations across the bone fragment, three separate fragments each from Bone A and Bone B were analyzed independently for amino acids. The procedure for proteins was as follows: 100 μL of a solution of 6 N HCl was added to the vials and heated for 24 h at 105 °C; then evaporated and reconstituted in 25 mM HCl to a final volume of 60 μL, mixed with 32 μL of ethanol, 8 μL pyridine, and 5 μL ECF, shaken for 5 s, and added to 100 μL 1% ECF in chloroform. The chloroform layer was transferred into a vial and the solution was extracted a second time, neutralized, concentrated, and injected into the GC/MS. An INNOWAX (25 M × 0.2 mm × 0.2 μm) capillary column was used for the separation. Helium carrier gas was set to a linear velocity of 38.8 cm/s, at 1 mL/min. Splitless injection was used with a 60 s purge off time, and was set to 240 °C. The MS transfer line was set to 240 °C. The GC oven temperature program was as follows: 70 °C for 1 min; 20 °C/min to 250 °C; isothermal for 3.5 min. Total run time was 12 min.

Protein Identification by Dot-Enzyme-Linked ImmunoSorbent Assays (Dot-ELISA). Elution buffer was prepared using 25 mM tris(hydroxymethyl)amino methane (TRIS), 6 M urea, 191 mM glycine, and 868 mM sodium dodecylsulfate (SDS). Phosphate saline buffer (PBS) was prepared using 1.37 M NaCl, 27 mM KCl, 100 mM Na_2HPO_4, and 14 mM KH_2PO_4. Blocking buffer was prepared using 0.2% (v/v) polyoxyethylene (20) sorbitan monolaurate (TWEEN 20) and 5% (w/v) nonfat dry milk (Oxoid, UK) in PBS (1.37 M NaCl, 27 mM KCl, 100 mM Na_2HPO_4, 14 mM KH_2PO_4). This was used as protein source for blocking nonspecific reactions, as an incubation medium, and for subsequent washing to remove unreacted reagents. The buffers were freshly prepared. All the reagents were analysis grade (>99.5% purity) and were purchased from Merck (Darmstadt, Germany). Enzyme substrate in tablet SIGMA FAST BCIP/NBT (5-bromo-4-chloro-3-indolyl phosphate/nitro blue tetrazolium) and rabbit anti-goat IgG alkaline phosphatase conjugate (1:5000 final concentration) antibodies were purchased from Sigma-Aldrich. Goat anti-collagen type I (1:2000 final concentration) was purchased from AbCam (Cambridge, UK). Methanol (GC purity >99.5%) was supplied by Merck.

RESULTS AND DISCUSSION

$Ca(OH)_2$ nanoparticles dispersed in 2-propanol (Nanorestore), specifically developed to consolidate carbonate matrices (i.e., wall paintings, carbonate stones)[29−33] and for the deacidification of cellulose based materials,[34,35] were used in this study for the consolidation of Late Middle Ages relics made of bone fragments. Once applied, $Ca(OH)_2$ nanoparticles react with atmospheric CO_2 in the presence of water to give $CaCO_3$: the new crystalline carbonate matrix formed in the original weakened porous substrate, acts both as binder and as a filler for areas affected by flaking, cracking phenomena, as well as by detachment of the surface. Then, this innovative nanostructured $Ca(OH)_2$-based method satisfies the following requirements: (i) capability to reinforce and harden fragile bones and stop flaking and powdering; (ii) good physical−chemical compatibility with the porous substrate; (iii) cost effectiveness; (iv) user-friendly employment. Moreover, the alkaline local character of $Ca(OH)_2$ nanoparticles dispersed in 2-propanol enhance the antimicrobiological activity and avoid all the undesired effects associated with the use of water based systems.

With collagen being the main protein constituting bone tissues, the presence of such protein within the bone fragments was expected and, as indicated in the Introduction, this should enhance the subsequent formation of aragonite after $Ca(OH)_2$ carbonation. Indeed, the presence of collagen within the bone fragments was ascertained by both GC-MS and Dot-ELISA analyses. Before the treatment by nanolime, some fragments of bone from the femur were collected as reference samples representative of the state of preservation of the skeleton before the treatment by $Ca(OH)_2$ nanomaterial. The same fragments characterized before the treatment were subjected to $Ca(OH)_2$ application according to the procedure reported in the Materials and Methods section. Both not treated (NT) and treated samples (T) were studied by means of several techniques in order to verify if aragonite phase was actually crystallized, conferring hardness to demineralized bone remains.

dx.doi.org/10.1021/la404085v | Langmuir 2014, 30, 660−668

Table 1. Amino Acid Composition in ppm of the Protein Component Present in the Two Bone Fragments

	amino acids (ppm)											
sample	alanine	glycine	valine	leucine	isoleucine	proline	serine	threonine	phenylalanine	hydroxyproline	amino acids	% amino acids
NT	4.4	10.6	1.0	1.5	0.6	5.0	0.8	0.6	0.8	3.7	29	1.1
NT	3.1	8.1	0.8	1.2	0.4	3.4	0.6	0.5	0.6	2.3	21	0.8
NT	11.5	16.8	2.6	4.1	1.3	12.5	2.3	1.4	2.3	11.3	66	2.6
T	5.1	11.3	1.2	1.8	0.7	5.7	0.2	0.6	0.2	4.0	31	1.0
T	8.9	15.8	2.1	2.8	1.0	10.4	0.3	1.2	0.3	8.3	53	1.7
T	6.6	13.2	1.6	2.3	0.8	8.2	1.0	0.8	1.0	5.6	41	1.3

Table 1 shows the amino acid composition of the protein contained in the two bone fragments: treated (T) and not treated (NT). The results are in agreement with the presence of collagen within the samples. The variation of amino acid content within the same series of samples was due to the intrinsic heterogeneous distribution of collagen within the bone fragments. It is not surprising that the bone fragments hundreds of years old still incorporated sufficient collagen fiber capable of inducing formation of aragonite needle crystals. Indeed, the relics have been conserved in a closed shrine that limited contact with external pathogenic agents, minimizing the degradation of the collagen. The Dot-ELISA test confirmed this finding as shown in Figure 1: the presence of collagen in

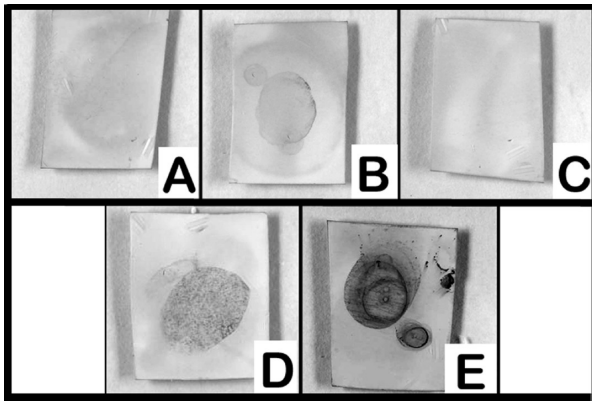

Figure 1. Color staining for Dot-ELISA tests: (A) blank; (B) pure collagen, positive test; (C) ovalbumin, negative test; (D) T bone fragments; (E) NT bone fragments.

the not treated (NT) sample was clearly evident, whereas in the treated sample the staining was less pronounced. This was due to the interaction between the collagen and the strong local alkalinity surrounding the $Ca(OH)_2$ nanoparticles possibly inducing partial denaturation of the protein. According to the literature[36] this phenomenon could be a potential drawback inducing deleterious effects for the bone integrity, due to the collagen hydrolysis in strongly alkaline environment. Indeed, there are two main reasons that allow us to exclude these deleterious effects: (i) the presence of 2-propanol instead of water as liquid medium, and (ii) the faster kinetics of the $Ca(OH)_2$ carbonation reaction[37] than the collagen hydrolysis process.[38] Dot-ELISA tests, carried out at complete carbonation and neutral pH, confirmed these different kinetics: in fact, they showed clear evidence of collagen, even with less pronounced staining. Therefore, the denaturation was absolutely only partial and completely under control. Furthermore, the ion chromatography data showed the presence of Mg^{2+} in traces (around 1000 ppm in both NT and T samples). This feature together with the detected collagen makes these bones a templating support that favors the crystallization of aragonite crystals.[17]

The mineralization action induced by carbonation of $Ca(OH)_2$ nanoparticles was clearly highlighted by microtomography imaging performed on NT and T samples. The demineralized bone surface (NT sample) was characterized by the presence of roughness, flakes, and thin layers of material weakly connected to the body underneath (Figure 2). No more

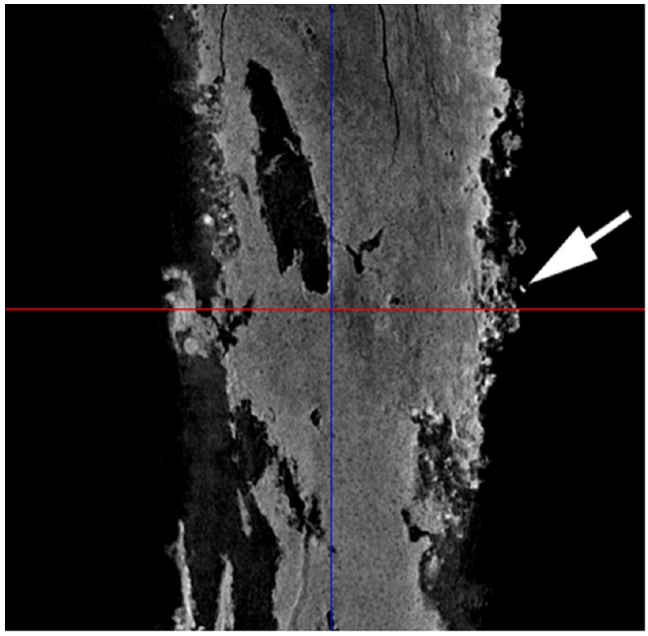

Figure 2. Microtomography image (section) of NT sample. The arrow indicates the front of the fragment.

flaking phenomena or powdering were identified after carbonation of the nanolime treatment: the surface appeared more compact while roughness disappeared (see Figure 3). ESEM and SEM images were collected on both not treated and treated pieces of bone with the aim of verifying the changes on the internal (*spongiosa*) and external surfaces and, above all, the shape and location of the crystals formed after carbonation. In particular, it was interesting to verify whether aragonite along with calcite was actually crystallized or not. Both surfaces of the not treated sample appeared homogeneously characterized by the presence of irregularly shaped and variably sized mineral bodies (Figure 4A and B), probably associated with flaking phenomena affecting the cortical bone layer (this phenomenon was particularly evident especially on the *spongiosa*; see Figure 4B). The presence of P and Ca in the EDS analysis (see Table 2, columns labeled as NT) was attributed to dahallite $Ca_5(PO_4, CO_3)_3$ (OH), the main mineral component of human bones,[3] as also confirmed by the XRD and FTIR analysis carried out on

dx.doi.org/10.1021/la404085v | *Langmuir* 2014, 30, 660−668

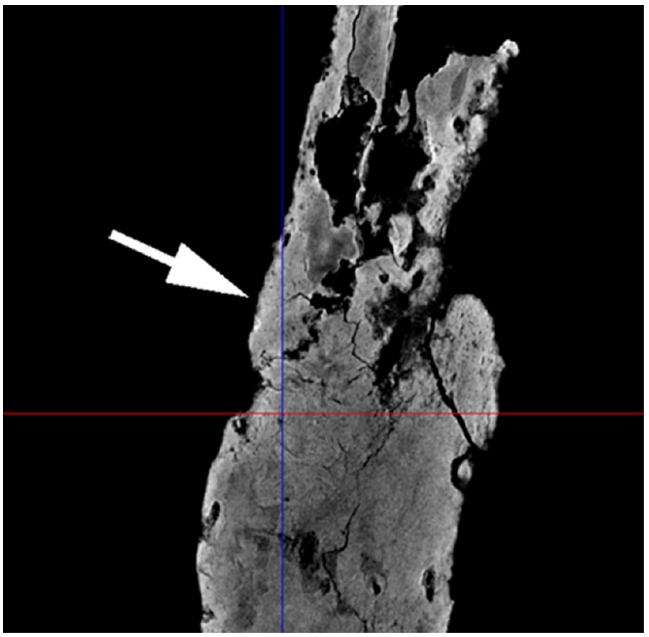

Figure 3. Microtomography image (section) of T sample. The arrow indicates the front of the fragment.

two samples obtained by grinding two bone fragments of the relic before and after the consolidation treatment (Figures 5 and 6, respectively). The reason neither aragonite nor calcite signals were detected in the XRD spectra is due to their low concentration, always below the detection limit, that as

Table 2. Elemental Analysis of the Bone of the Relic before (columns NT) and after (columns T) the Consolidation Treatment Carried Out Both on the Front (F) and on the Rear (R) of the Fragments by Application of the $Ca(OH)_2$ Nanoparticles[a]

	NT (At %)		T (At %)			
	F	R	F		R	
Element			Points 1	Points 2	Points 1	Points 2
C	16.3	32.2	17.7	31.1	31	35.3
O	57.6	49	30.1	48.1	43	53.5
Na	/	0.8	/	/	/	/
Mg	/	0.9	7.7	/	/	/
Al	/	3.8	1.9	2	/	/
Si	1.9	6.7	1.5	3.9	/	/
P	7.7	1.4	13.6	2.8	/	/
K	/	1.6	6.5	/	3.9	/
Ca	16.6	3.4	20.1	11.3	22.5	10.1

[a]Slash (/) indicates that the corresponding element has not be detected.

indicated by Kontoyannis et al.[39] is 0.9 w/w% and 2.6 w/w%, respectively, for calcite and aragonite. It is worthwhile to mention that the integral intensity of the pattern corresponding to T sample (red) was reduced due to the lower amount of sample available for the XRD measurements. Taking into account the procedure for the quantitative analysis of both calcite and aragonite based on FTIR spectroscopy,[40] we calculated the total amount of these two minerals, obtaining for both concentration values below 0.1 w/w% (and then well

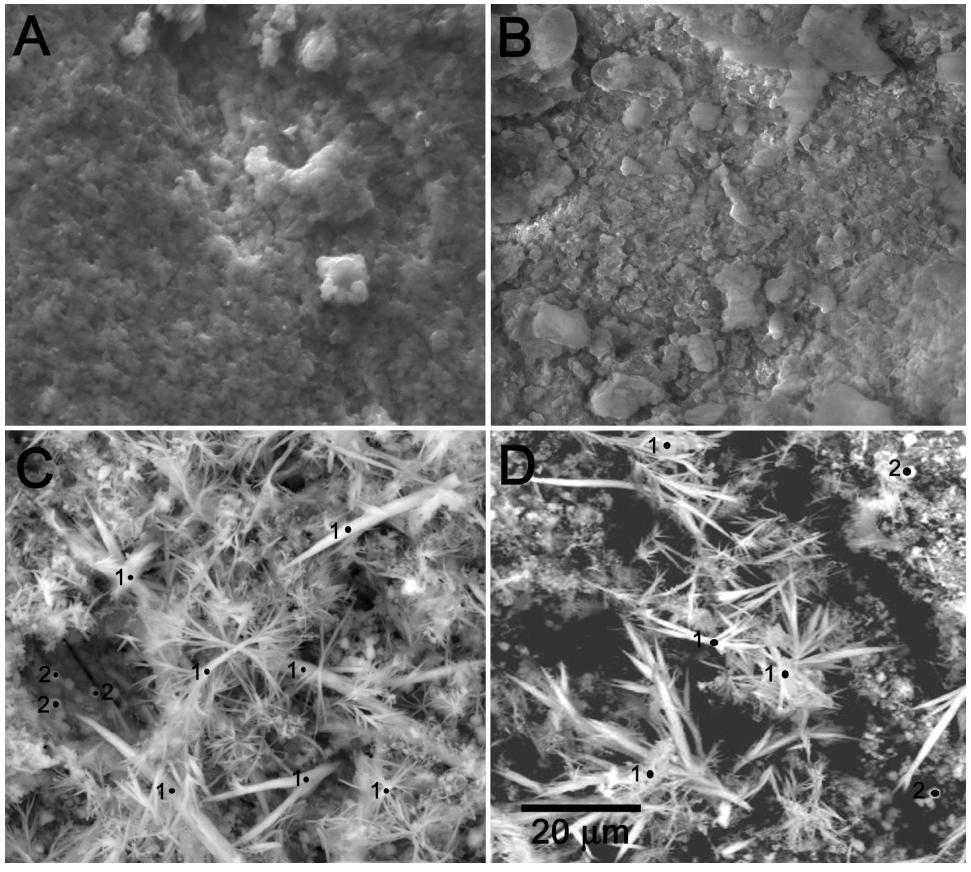

Figure 4. ESEM micrographs of external (A) and internal (B) NT sample surface, and of the external (C) and internal (D) T sample surface.

dx.doi.org/10.1021/la404085v | *Langmuir* 2014, 30, 660−668

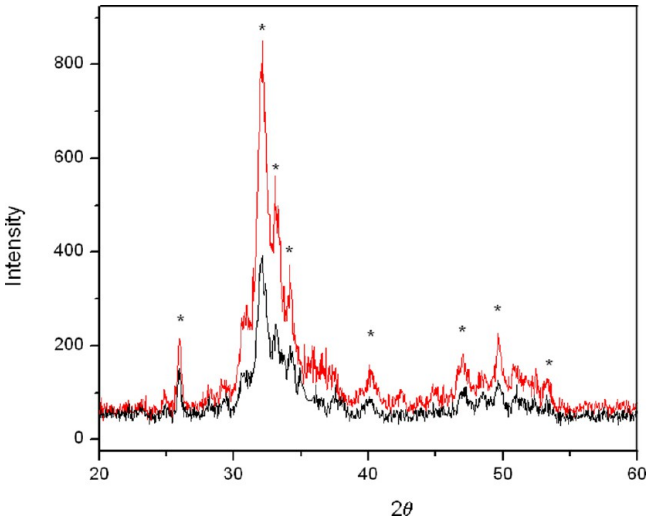

Figure 5. XRD patterns collected onto (red) NT sample and (black) T sample. * indicates the peaks typical of hydroxyapatite.

below the XRD detection limit). By contrast, the micrographs collected on the internal and external surfaces of the treated sample highlighted the presence of needle-like crystals, the characteristic shape of aragonite,[38] on both sides of the sample (Figure 4C and D). In order to obtain information about the chemical nature of these crystals, morphologically attributed to aragonite, many spot-sized elemental analyses were carried out on different points of the treated bone by means of EDS probe (these points have been labeled 1; see Figure 4C and D); the average composition is reported in Table 2 (see columns labeled as T). It is evident that these crystals, besides carbon and oxygen (Figure 4B), contained only Ca. This feature, together with the comparison of their morphology with that of aragonite,[33,34] suggested that the carbonated needle-shaped phase formed could reasonably be aragonite, which may crystallize in such a shape, as indicated by many authors.[41,42]

A further feature of the micrographs in Figure 4C and D is the presence of polyedric crystals (labeled 2); their average elemental composition (also in this case the EDS spot-sized elemental analyses detected only the presence of O, C, and Ca; see columns T, Points 2, Table 2) together with their morphology indicated that they are composed of calcite.

FTIR analysis was performed to verify whether differences in the absorbance spectra of NT and T samples were detectable. A comparison of the two spectra of NT (red line) and T (black line) samples is shown in Figure 6. The spectrum of the consolidated bone, in addition to the peaks typical of calcite and dahallite (see Supporting Information Figure SI2), clearly showed the presence of a shoulder at 855 cm^{-1} (out-of-plane bending mode of the O−C−O bond of the CO_3^{2-} anion) and of a peak at 700 cm^{-1} (in-plane bending mode of the O−C−O bond of the CO_3^{2-} anion) that, as indicated in the literature,[43] are attributable to the presence of aragonite (see black spectra in Figure 6A and B respectively), confirming the attribution made by morphological features detected by ESEM and EDS. Therefore, FTIR data enabled us to conclude that calcite was present even before the treatment and this was possibly due to past conservation treatment made by using $(NH_4)_2CO_3$ solution, which is a quite common practice. On the other hand, the treatment by nanolime and subsequent carbonation process led to the increase of calcite content (see Supporting Information Figure SI2) and to the freshly formed aragonite.

In order to investigate the effects induced by the $Ca(OH)_2$ nanoparticle application in strengthening bones, Vickers microhardness tests were performed on both NT and T samples. The results shown in Table 3 indicate an enhancement

Table 3. Vickers Microhardness Results of NT and T Samples

sample	mean value (Gpa)	std. dev. (Gpa)	min. value (Gpa)	max value (Gpa)
NT	0.6	0.3	0.3	1.2
T	2.2	0.2	1.9	2.5

of the hardness that the treatment increases by almost 3.5 times. This strong effect was attributed to the formation of aragonite inside the porous matrix constituting the bone (as confirmed by FTIR and ESEM measurements). As a matter of fact, Vickers microhardness of aragonite (2.25 GPa) is almost 30% higher than that of calcite (1.54 GPa).[44] Furthermore, the decrease of the standard deviation (Table 3) confirms that the application of $Ca(OH)_2$ nanoparticles led to the formation of a more uniform superficial layer with respect to the one observed on the NT sample. Furthermore, the reduction of porosity (η) of about 65% between the NT (η = 0.1775) and T (η = 0.0607)

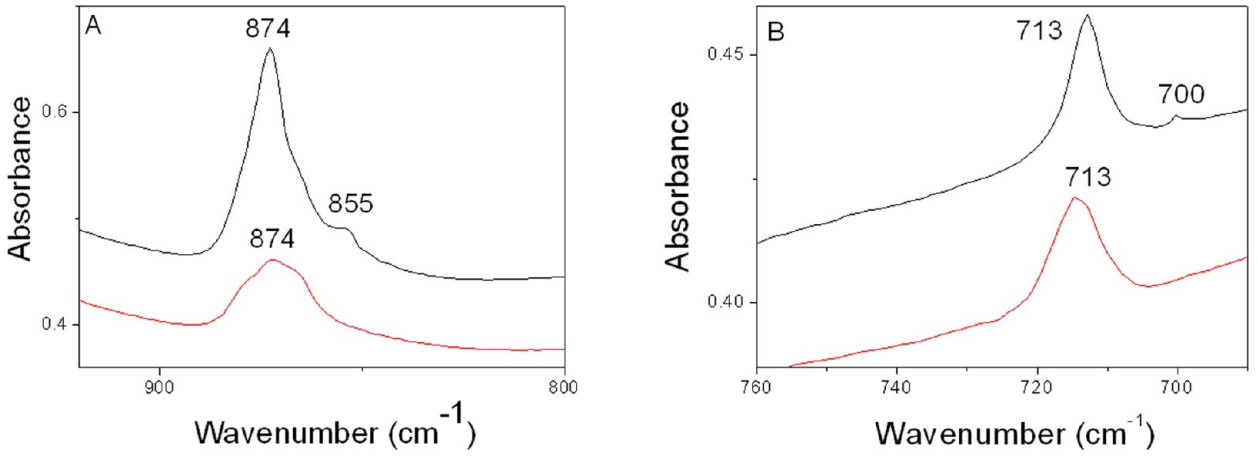

Figure 6. FTIR spectra of microsamples of the bones collected before (NT sample, red line) and after (T sample, black line) the application of $Ca(OH)_2$ nanoparticles and successive carbonation: (a) enlargement of the range 920−800 cm^{-1}; (b) enlargement of the range 770−680 cm^{-1}.

dx.doi.org/10.1021/la404085v | Langmuir 2014, 30, 660−668

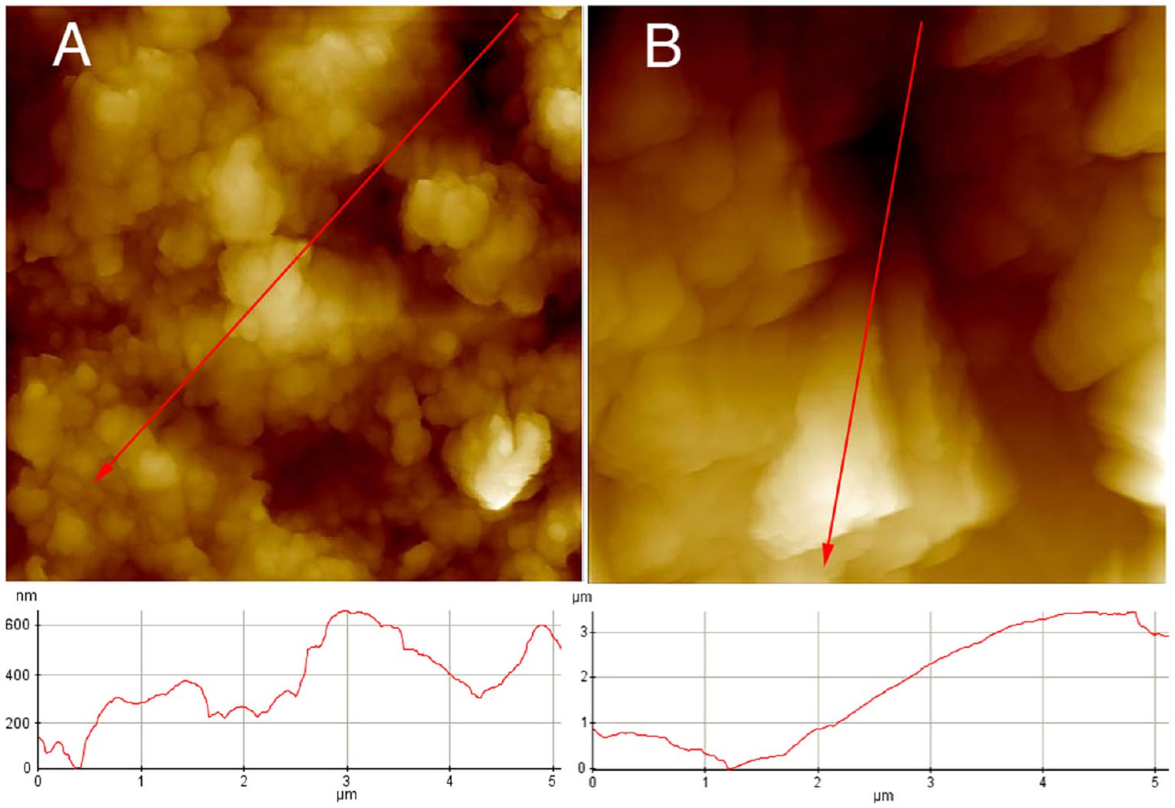

Figure 7. Top: 5 × 5 μm^2 AFM images of NT sample (A) and T sample (B). Bottom: trend of the *z*-range for NT (A) and (B) T sample.

samples indicated that aragonite crystallization occurred not only on the bone surface, but also within the pores, carrying out a remineralizing action inside the bone tissue. Then, crystals of aragonite formed both on the surface and in the porous structure, filling the pores, conferring compactness to demineralized bone tissue, and increasing the whole volume of the treated skeleton. This strong reduction of the porosity observed after the nanolime application is attributable to the fact that the treatment mostly involved the surface layers of the bone, causing occlusion of part of the open pores. This effect, monitored through He porosimetry, results in a decrease of the total porosity of the samples upon the application of the dispersion of $Ca(OH)_2$ nanoparticles in 2-propanol and successive carbonation.

Further evidence about the morphology and surface properties of the two samples was obtained by atomic force microscopy (AFM). Figure 6A, B refers to the topography of NT and T samples, respectively. The difference in the *z*-range between the two micrographs (0−890 nm for NT sample, Figure 7A bottom; and 0−3.25 μm for the T sample, Figure 7B bottom) and the topographic differences showed the presence of particles on the surface of the second one. In addition, AFM micrographs were used to calculate the root-mean-square roughness R_q following the procedure described in the Materials and Methods section and in Figure SI2. Results indicate a drastic reduction of the surface roughness (from 245 ± 20 nm for NT to 49 ± 5 nm for T sample), confirming a flattening of the surface, as previously stated from both hardness (Table 3) and tomography measurements (Figures 2 and 3).

CONCLUSIONS

In this study, aragonite crystals, a metastable polymorph of $CaCO_3$, were grown from nanostructured $Ca(OH)_2$ by reaction with atmospheric CO_2 exploiting the presence of collagen as template onto which the crystals are slowly formed during carbonation. $Ca(OH)_2$ nanoparticles dispersed in 2-propanol were applied onto the surface of demineralized bone remains. The carbonation process occurred and a controlled crystallization into aragonite phase was observed by means of scanning electron microscopy and Fourier transform infrared spectroscopy. Needle-shaped crystals were shown to crystallize onto bone surfaces, especially onto the back side (*spongiosa*); the comparison between spectra of not treated sample (NT) and treated sample (T) indicated the presence of aragonite as a newly formed mineralogical phase by the distinctive peak at 700 cm^{-1} (bending O−C−O of aragonite calcium carbonate).

The effectiveness in consolidating bones was evaluated by cross-checking results obtained with microtomography, helium porosimetry, Vickers microhardness test, and atomic force microscopy. Flaking phenomena and powdering were not detectable after the carbonation of nanostructured $Ca(OH)_2$, leading to a more compact and smooth surface. Moreover, the data suggest that the crystallization occurred not only on the bone surface (where a smooth film of aragonite was identified) but also inside pores, reducing porosity values and conferring hardness to the bone tissue. Implications of this study in the field of a new method for bone remediation in archeology and paleontology were also taken into account.

dx.doi.org/10.1021/la404085v | *Langmuir* 2014, 30, 660−668

■ ASSOCIATED CONTENT

Supporting Information

Additional figures as described in the text. This material is available free of charge via the Internet at http://pubs.acs.org.

■ AUTHOR INFORMATION

Corresponding Author

*E-mail: luigi.dei@unifi.it.

Present Address

Irene Natali, CNR-ISAC, Area della Ricerca CNR, via Gobetti 101, I-40129 Bologna, Italy.

Author Contributions

‡Stefania Sansoni, private conservator, via Galeno 6, 20126 Milan, Italy.

Notes

The authors declare no competing financial interest.

■ ACKNOWLEDGMENTS

Authors express their gratitude to Drs. Francesca Loglio and Samuele Ciattini (CRIST − Centro di Cristallografia Strutturale, University of Florence), Dr. Mario Paolieri and Mr. Maurizio Ulivi (M.E.M.A. − Centro Interdipartimentale di Microscopia Elettronica e Microanalisi, University of Florence), Dr. Rita Traversi (Chemistry Department, University of Florence), and Michael Schilling and Joy Mazurek (The Getty Conservation Institute) for their assistance, stimulating discussions and comments during the microtomography, SEM-EDS, ion chromatography, and GC-MS measurements, respectively. Dr. Assunta Sfalanga (Centro di Geotecnologie, University of Siena) is also thanked for performing the helium porosimetry experiments. Financial support from Consorzio interuniversitario per lo sviluppo dei Sistemi a Grande Interfase (CSGI), Florence, Italy, and from the University of Florence Fondi d'Ateneo ex-60% is gratefully acknowledged. Financial support from the Tuscany Region, Italy, TemArt Project European Fund for Regional Development (POR CreO FESR 2007-2013) and SICAMOR Project PAR-FAS Tuscany region is also acknowledged.

■ REFERENCES

(1) Dorozhkin, S. V.; Epple, M. Biological and medical significance of calcium phosphates. *Angew. Chem., Int. Ed.* **2002**, *41*, 3130−3146.

(2) Lakes, R. Materials with structural hierarchy. *Nature* **1993**, *361*, 511−515.

(3) Weiner, S.; Wagner, H. D. The material bone: Structure mechanical function relations. *Annu. Rev. Mater. Sci.* **1998**, *28*, 271−298.

(4) Meyers, M. A.; Chen, P.-Y.; Lin, A.Y-M.; Seki, Y. Biological materials: structure and mechanical properties. *Progr. Mater. Sci.* **2008**, *53*, 1−206.

(5) Currey, J. D. Physical characteristics affecting the tensile failure properties of compact bone. *J. Biomech.* **1990**, *23* (8), 837−844.

(6) Osteoporosis and osteomalacia. In *Harrison's Manual of Medicine*; Fauci, A., Braunwald, E., Kasper, D., Hauser, S., Longo, D., Jameson, J., Loscalzo, J., Eds.; Mc Graw Hill Medicine: USA, 2009; pp 965−967.

(7) Gonzalez-Reimers, E.; Velasco-Vazquez, J.; Arnay-de-la-Rosa, M.; Machado-Calvo, M. Quantitative computerized tomography for the diagnosis of osteopenia in prehistoric skeletal remains. *J. Archaeol. Sci.* **2007**, *34*, 554−561.

(8) Farquharson, M. J.; Speller, R. D.; Brickley, M. Measuring bone mineral density in archaeological bone using energy dispersive low angle X-ray scattering techniques. *J. Archaeol. Sci.* **1997**, *24*, 765−772.

(9) Berna, F.; Matthews, A.; Weiner, S. Solubilities of bone mineral from archaeological sites: the recrystallization window. *J. Archaeol. Sci.* **2004**, *31*, 867−882.

(10) Hiller, J. C.; Wess, T. J. The use of small-angle X-ray scattering to study *archaeological* and experimentally altered bone. *J. Archaeol. Sci.* **2006**, *33*, 560−572.

(11) Piga, G.; Santos-Cubedo, A.; Brunetti, A.; Piccinini, M.; Malgosa, A.; Napolitano, E.; Enzo, S. A multi-technique approach by XRD, XRF, FT-IR to characterize the diagenesis of dinosaur bones from Spain. *Palaeogeogr., Palaeoclim., Palaeoecol.* **2011**, *310*, 92−107.

(12) Lebon, M.; Reiche, I.; Bahain, J.-J.; Chadefaux, C.; Moigne, A.-M.; Fröhlich, F.; Sémah, F.; Schwarcz, H. P.; Falguères, C. New parameters for the characterization of diagenetic alterations and heat-induced changes of fossil bone mineral using Fourier transform infrared spectrometry. *J. Archaeol. Sci.* **2010**, *37*, 2265−2276.

(13) Alfano, D.; Albunia, A. R.; Motta, O.; Proto, A. Detection of diagenetic alterations by spectroscopic on archaeological bones from the Necropolis of Poseidonia (Paestum): a case study. *J. Cult. Herit.* **2009**, *10*, 509−513.

(14) Zylberberg, L.; Laurin, M. C. R. Analysis of fossil bone organic matrix by transmission electron microscopy. *Palevol* **2011**, *10*, 357−366.

(15) López-Polín, L. Possible interferences of some conservation treatments with subsequent studies on fossil bones: A conservator's overview. *Quat. Int.* **2012**, *275*, 120−127.

(16) Reddy, M. M.; Wang, K. K. Crystallization of calcium carbonate in the presence of metal ions: I. Inhibition by magnesium ion at pH 8.8 and 25 C. *J. Cryst. Growth* **1980**, *50*, 470−480.

(17) Jiao, Y.; Feng, Q.; Li, X. The Co-effect of collagen and magnesium ions on calcium carbonate biomineralization. *Mater. Sci. Eng., C* **2006**, *26*, 648−652.

(18) Falini, G.; Fermani, S.; Gazzano, M.; Ripamonti, A. Calcite crystallization on gelatin films containing polyelectrolytes. *Chem.—Eur. J.* **1997**, *3*, 1807−1814.

(19) Weissbuch, I.; Addadi, L.; Lahav, M.; Leiserowitz, L. Molecular recognition at crystal interfaces. *Science* **1991**, *253*, 637−645.

(20) Mann, S.; Archibald, D. D.; Didymus, J. M.; Douglas, T.; Heywood, B. R.; Meldrum, F. C.; Reeves, N. J. Crystallization at inorganic-organic interfaces: biominerals and biomimetic synthesis. *Science* **1993**, *261*, 1286−92.

(21) Belcher, A. M.; Wu, X. H.; Christensen, R. J.; Hansma, P. K.; Stucky, G. D.; Morse, D. E. Control of crystal phase switching and orientation by soluble mollusc-shell proteins. *Nature* **1996**, *381*, 56−58.

(22) Thomposon, J .B.; Paloczi, G. T.; Kindt, J. H.; Michenfelder, M.; Smith, B. L.; Stucky, G.; Morse, D .E.; Hansma, P. K. Direct observation of the transition from calcite to aragonite growth as induced by abalone shell proteins. *Biophys. J.* **2000**, *79*, 3307−3312.

(23) Shen, F. H.; Feng, Q. L.; Wang, C. M. The modulation of collagen on crystal morphology of calcium carbonate. *J. Cryst. Growth* **2002**, *242*, 239−244.

(24) Gomez-Villaba, L. S.; López-Arce, P.; Alvarez de Buergo, M.; Fort, R. Atomic defects and their relationship to aragonite−calcite transformation in portlandite nanocrystal carbonation. *Cryst Growth Des.* **2012**, *12*, 4844−4852.

(25) Litvin, A. L.; Valiyaveettil, S.; Kaplan, D. L.; Mann, S. Template-directed synthesis of aragonite under supramolecular hydrogen-bonded langmuir monolayers. *Adv. Mater.* **1997**, *9*, 124−127.

(26) Aizenberg, J.; Weaver, J. C.; Thanawala, M. S.; Sundar, V. C.; Morse, D. E.; Fratzl, P. Skeleton of *Euplectella* sp.: structural hierarchy from the nanoscale to the macroscale. *Science* **2005**, *309*, 275−278.

(27) Nanni, A.; Dei, L. $Ca(OH)_2$ nanoparticles. from W/O microemulsions. *Langmuir* **2003**, *19*, 933−938.

(28) Salvadori, B.; Dei, L. Synthesis of $Ca(OH)_2$ nanoparticles from diols. *Langmuir* **2001**, *17*, 2371−2374.

(29) Natali, I.; Saladino, M. L.; Andriulo, F.; Chillura Martino, D.; Caponetti, E.; Carretti, E.; Dei, L. Consolidation and protection by nanolime: Recent advances for the conservation of the graffiti, Carceri dello Steri Palermo and of the 18th century lunettes, SS. Giuda e

Simone Cloister, Corniola (Empoli). *J. Cult. Herit.* **2013**, http://dx.doi.org/10.1016/j.culher.2013.03.002.
(30) Giorgi, R.; Bozzi, C.; Dei, L.; Gabbiani, C.; Ninham, B. W.; Baglioni, P. Nanoparticles of $Mg(OH)_2$: synthesis and application to paper conservation. *Langmuir* **2005**, *21*, 8495−8501.
(31) Ambrosi, M.; Dei, L.; Giorgi, R.; Neto, C.; Baglioni, P. Colloidal particles of $Ca(OH)_2$: properties and application to restoration of frescoes. *Langmuir* **2001**, *17*, 4251−4255.
(32) Drdácký, M.; Slížková, Z.; Ziegenbalg, G. A nano approach to consolidation of degraded historic lime mortars. *J. Nano Res.* **2009**, *8*, 13−22.
(33) Daniele, V.; Taglieri, G. Synthesis of $Ca(OH)_2$ nanoparticles with the addition of Triton X-100. Protective treatments on natural stones: Preliminary results. *J. Cult. Herit.* **2012**, *13*, 40−46.
(34) Giorgi, R.; Dei, L.; Ceccato, M.; Schettino, C.; Baglioni, P. Nanotechnologies for conservation of Cultural Heritage: paper and canvas deacidification. *Langmuir* **2002**, *18*, 8198−8203.
(35) Poggi, G.; Giorgi, R.; Toccafondi, N.; Katzur, V.; Baglioni, P. Hydroxide nanoparticles for deacidification and concomitant inhibition of iron-gall ink corrosion of paper. *Langmuir* **2010**, *24*, 19084−19090.
(36) Collins, M. J.; Nielsen-Marsh, C. M.; Hiller, J.; Smith, C. I.; Roberts, J. P.; Prigodich, R. V.; Wess, T. J.; Csapò, J.; Millard, A. R.; Turner-Walker, G. The survival of organic matter in bone: a review. *Archaeometry* **2002**, *44*, 383−394.
(37) Carretti, E.; Chelazzi, D.; Rocchigiani, G.; Baglioni, P.; Poggi, G.; Dei, L. Interactions between nanostructured calcium hydroxide and acrylate copolymers: implications in cultural heritage conservation. *Langmuir* **2013**, *29*, 9881−9890.
(38) Collins, M. J. A basic mathematical simulation of the chemical degradation of ancient collagen. *J. Archaeol. Sci.* **1995**, *22*, 175−183.
(39) Kontoyannis, C. G.; Vagenas, N. V. Calcium carbonate phase analysis using XRD and FT-Raman spectroscopy. *Analyst* **2000**, *125*, 251−255.
(40) Vagenas, N. V.; Gatsouli, A.; Kontoyannis, C. G. Quantitative analysis of synthetic calcium carbonate polymorphs using FT-IR spectroscopy. *Talanta* **2003**, *59*, 831−836.
(41) Hu, Z.; Shao, M.; Cai, Q.; Ding, S.; Zhong, C.; Wei, X.; Deng, Y. Synthesis of needle-like aragonite from limestone in the presence of magnesium chloride. *J. Mater. Process. Technol.* **2009**, *209*, 1607−1611.
(42) Wang, L.; Sondi, I.; Matijević, E. Preparation of uniform needle-like aragonite particles by homogeneous precipitation. *J. Colloid Interface Sci.* **1999**, *218*, 545−553.
(43) Rizzuti, A.; Leonelli, C. Crystallization of aragonite particles from solution under microwave irradiation. *Powder Technol.* **2008**, *186*, 255−262.
(44) http://www.cidraprecisionservices.com/mohs-conversion.html (accessed Jan. 3rd, 2014).